

INNOVATIVE METHODOLOGY

Robotic navigation to subcortical neural tissue for intracellular electrophysiology in vivo

W. A. Stoy,¹ I. Kolb,¹ G. L. Holst,² Y. Liew,¹ A. Pala,¹ B. Yang,² E. S. Boyden,^{3,4}
G. B. Stanley,¹ and C. R. Forest^{1,2}

¹Wallace H. Coulter Department of Biomedical Engineering, Georgia Institute of Technology, Atlanta, Georgia; ²George W. Woodruff School of Mechanical Engineering, Georgia Institute of Technology, Atlanta, Georgia; ³Media Lab, Massachusetts Institute of Technology, Cambridge, Massachusetts; and ⁴McGovern Institute for Brain Research, Massachusetts Institute of Technology, Cambridge, Massachusetts

Submitted 21 February 2017; accepted in final form 25 May 2017

Stoy WA, Kolb I, Holst GL, Liew Y, Pala A, Yang B, Boyden ES, Stanley GB, Forest CR. Robotic navigation to subcortical neural tissue for intracellular electrophysiology in vivo. *J Neurophysiol* 118: 1141–1150, 2017. First published June 7, 2017; doi:10.1152/jn.00117.2017.—In vivo studies of neurophysiology using the whole cell patch-clamp technique enable exquisite access to both intracellular dynamics and cytosol of cells in the living brain but are underrepresented in deep subcortical nuclei because of fouling of the sensitive electrode tip. We have developed an autonomous method to navigate electrodes around obstacles such as blood vessels after identifying them as a source of contamination during regional pipette localization (RPL) in vivo. In mice, robotic navigation prevented fouling of the electrode tip, increasing RPL success probability 3 mm below the pial surface to 82% ($n = 72/88$) over traditional, linear localization (25%, $n = 24/95$), and resulted in high-quality thalamic whole cell recordings with average access resistance (32.0 M Ω) and resting membrane potential (–62.9 mV) similar to cortical recordings in isoflurane-anesthetized mice. Whole cell yield improved from 1% ($n = 1/95$) to 10% ($n = 9/88$) when robotic navigation was used during RPL. This method opens the door to whole cell studies in deep subcortical nuclei, including multimodal cell typing and studies of long-range circuits.

NEW & NOTEWORTHY This work represents an automated method for accessing subcortical neural tissue for intracellular electrophysiology in vivo. We have implemented a novel algorithm to detect obstructions during regional pipette localization and move around them while minimizing lateral displacement within brain tissue. This approach leverages computer control of pressure, manipulator position, and impedance measurements to create a closed-loop platform for pipette navigation in vivo. This technique enables whole cell patching studies to be performed throughout the living brain.

in vivo; patch clamp; subcortical; thalamus; whole cell recording

IN VIVO PATCH-CLAMP RECORDING is one of the most important and versatile techniques in neuroscience. Whole cell recordings have enabled stable investigation of subthreshold activity to identify cell types and circuits in the intact brain. This technique is also uniquely positioned to enable concurrent measurements of intrinsic and sensory evoked electrophysiology in either voltage- or current-clamp mode (Constantinople and Bruno 2013; Harvey et al. 2009), morphology (Margrie et

al. 2002), and the genetic profile of single neurons (Cadwell et al. 2016), as well as the ability to introduce foreign genetic material into the cell (Rancz et al. 2011; Vélez-Fort et al. 2014). There is growing interest in multimodal cell type classification (electrophysiological, morphological, and/or genetic, etc.) throughout the brain, a major goal of the Brain Research through Advancing Innovative Neurotechnologies (BRAIN) Initiative (Bargmann and Newsome 2014). Although recently developed genetic voltage indicators have been used with some success to measure activity from both individual neurons and populations (Lin and Schnitzer 2016), the heterogeneous tissue of the brain acts as a scattering medium, limiting recordings to superficial cortical layers in the mammalian brain. Sharp intracellular recording techniques similarly have subthreshold resolution but suffer from short recording times (Fee 2000) and are unsuitable for voltage-clamp recordings because of high electrode impedance.

While whole cell patch clamping is the gold standard for in vivo electrophysiology, it requires skill to perform and has thus been more extensively used for in vitro experiments. Recent efforts to automate it have been productive, yet subcortical recording with whole cell patch clamping remains a low-yield endeavor. Published papers are scant (Brecht and Sakmann 2002; Groh et al. 2014; Margrie et al. 2002), but whole cell recordings in deep subcortical nuclei are difficult to obtain and are known to suffer from increased access resistance (Margrie et al. 2002). In a literature review of the 60 most-cited papers that reported low-access resistance, blind, whole cell recordings in vivo, only 5% of all 2,350 recorded cells were recorded at depths exceeding 3 mm from the pial surface in rodents. Several other studies have demonstrated recordings in the cat thalamus in vivo (several centimeters below the pial surface) but report high access resistance of the electrodes (Wang et al. 2007, 2011).

To investigate these subcortical nuclei in vivo, researchers have used extracellular, juxtасomal, cell-attached, or sharp intracellular recordings (Friedberg et al. 2004; Higley and Contreras 2007; Petersen et al. 2008; Polack and Charpier 2006; Wang et al. 2010a; Yu et al. 2004), indicating that deep whole cell recordings, while valuable and desirable, are exceedingly difficult to obtain. To enable this important tech-

Address for reprint requests and other correspondence: C. R. Forest, Georgia Inst. of Technology, Atlanta GA 30332 (e-mail: cforest@gatech.edu).

nique to be used throughout the brain, we identify a need to improve both the yield and quality of deep whole cell recordings.

It is well known that a pipette must be clean, with a good tip geometry, to enable formation of a gigaseal with a target cell (Neher 1997). Since deep recording requires traversing through several millimeters or centimeters of heterogeneous tissue (e.g., blood vessels, glial cells, membranes) to reach a region of interest during regional pipette localization (RPL), the pipette invariably encounters, and is clogged by, debris from this tissue. Efforts to date to mitigate this problem have had limited success. In their 2002 study, Margrie et al. suggested that increasing pipette pressure or advancing the pipette through a guide tube may reduce access resistance (or equivalently, increase quality) (Margrie et al. 2002). However, Brecht and Sakmann (2002) subsequently noted that neither higher pressures nor a guide tube reduced the access resistance of thalamic recordings.

We set out to investigate the relationship between this troublesome first stage of patch clamping, RPL, and high-access resistance, low-yield whole cell experiments. By attempting whole cell trials in the mouse thalamus, a deep brain structure of wide interest (Kelly et al. 2014; Llinás and Steriade 2006; Sherman 2005), we observed that transient high-amplitude fluctuations in resistance that occur during RPL are often followed by residual, permanent increases in pipette tip resistance, preventing successful whole cell recordings, and that these obstructions could be avoided with a series of small lateral movements, confirming previous observations by Lee et al. (2014) (see Fig. 1). By visualizing this process in slices of brain tissue on a microscope, we show that pipette penetration of blood vessels and the residue left on pipette tips are the likely cause of these resistance changes, along with meninges (dura, pia, and hippocampal meninges). Lateral steps enabled navigation around blood vessels and other obstacles without a residual increase in resistance, and meninges were penetrated with short, rapid plunges with the pipette. We developed an efficient algorithm for laterally moving around obstructing blood vessels during RPL *in vivo* and compared its effectiveness to linear localization. We found that whole cell trials performed 3 mm deep could be localized with the same yield

as we had previously demonstrated in the cortex (up to 1 mm) with direct linear localization and, in addition, had access resistances comparable to whole cell recordings performed previously in the cortex.

MATERIALS AND METHODS

Acute in Vivo and in Vitro Preparation

All experimental protocols were approved by the Georgia Tech Institutional Animal Care and Use Committee. For *in vivo* preparation, all mice ($n = 19$) were prepared for acute experimentation as we have done previously (Kodandaramaiah et al. 2012). Briefly, young male C57BL/6 mice [postnatal day (P)35–P49] were anesthetized with isoflurane and headfixed to a titanium headplate with C&B-Metabond dental cement (Parkell, Edgewood, NY). Craniotomies (1-mm diameter) and duratomies were performed above the ventral posteromedial nucleus (VPM) of the thalamus (1.75 mm rostral, 1.75 mm lateral, 3 mm below the pial surface) with the use of stereotaxic coordinates from the Paxinos and Franklin mouse brain atlas (Paxinos and Franklin 2012).

For *in vitro* preparation, acute brain slices of mouse visual area V1 were prepared from male C57BL/6 adult mice (aged P30–P60) with the protective recovery method described in detail elsewhere (Wu et al. 2016).

Pipette Fabrication

Long-taper patch pipettes (e.g., 7 mm) were pulled from fire-polished borosilicate glass (BF150-86-10HP, Sutter Instrument, Novato, CA) on a P-1000 electrode puller with a 4.5-mm-wide box filament (Sutter Instrument). The long taper is achieved with an initial high-velocity step (heat = ramp + 10, velocity = 40), with subsequent steps used to develop the taper to $\sim 1 \mu\text{m}$ (3–4 pulls of heat = ramp – 10, velocity = 20).

Electrophysiology

Whole cell patch clamping was performed as described previously (Kodandaramaiah et al. 2016). In brief, an Autopatch 1500 (Neuromatic Devices, Atlanta GA) was used to provide computer-controlled pressure and measure resistance for both *in vitro* and *in vivo* experiments. Both *in vitro* and *in vivo* experiments used Multi-clamp 700B amplifiers (Molecular Devices, Sunnyvale, CA), and signals were digitized at 20 kHz with National Instruments DAQs

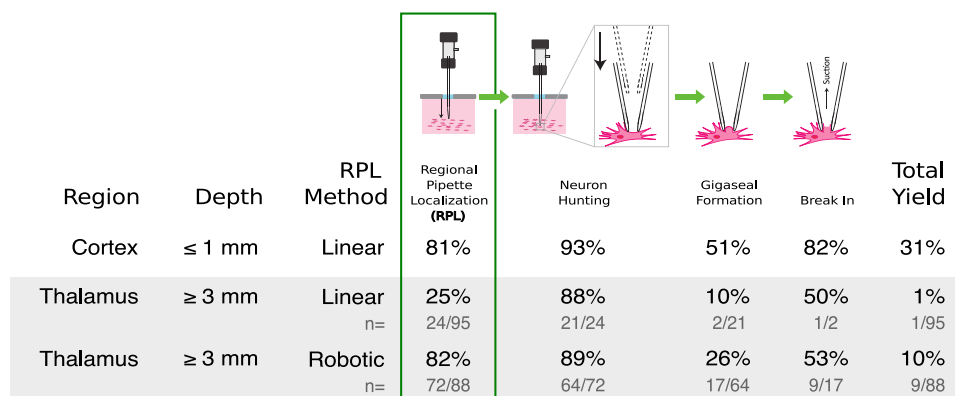


Fig. 1. Increased yield of regional pipette localization (RPL) during whole cell patching *in vivo* with robotic navigation. *In vivo* whole cell recording is a serial process consisting of RPL, neuron hunting, gigaseal formation, and break-in. Whole cell recording yield (total yield) is a linear product of previous success rates. During traditional linear localization, cortical (*top*) and thalamic (*middle*) pipettes are clogged in 1/5 insertions and 3/4 insertions, respectively, preventing further steps. The gray box indicates procedures presented in this study. The percentage of pipettes that successfully performed RPL increased from 25% to 82% and total whole cell yield increased from 1% to 10% when robotic navigation was performed. (Top row data reproduced from Kodandaramaiah et al. 2012 with permission.)

(in vivo DAQ: cDAQ-9174 and NI 9215, in vitro DAQ: NI USB-6221, National Instruments, Austin, TX) and recorded in pCLAMP 10 (Molecular Devices). A Slicescope Pro 1000 (Scientifica) was used to perform in vitro recordings, and an MP-285 micromanipulator (Sutter Instrument) with a PT1-Z8 Motorized Translation Stage (Thorlabs, Newton, NJ) was used for positioning the electrode for in vivo patch clamping.

Resistance measurements were performed throughout pipette translation, rather than only before and after translation as in our prior work (Kodandaramaiah et al. 2012, 2016). During pipette translation, starting from artificial cerebrospinal fluid (ACSF) on the surface of the tissue, resistance was recorded by applying a 20-mV-amplitude, 128-Hz square wave (50% duty cycle) to the pipette and calculating the resistance with Ohm's law. The resistance was computed as a moving average of four measurements (low-pass filter with 4 sample rectangular window). Thus filtered resistances were saved to an array, called the resistance array.

Blood Vessel Penetration

In addition to mapping a blood vessel in neural tissue with scanning ion conductance microscopy (SICM), we measured the resistance changes encountered as the pipette was translated through a blood vessel in vitro. The pipette was filled with ACSF and pressurized to high positive pressure (1,000 mbar) to replicate typical parameters for in vivo pipette localization (Kodandaramaiah et al. 2016). For this penetration experiment, the pipette was positioned above a blood vessel visually, at 35° relative to the image plane. The pipette was manually lowered until the tip resistance increased by 12.5% above initial pipette resistance and then retracted 15 μm to a starting position. Resistance was recorded while the pipette was manually advanced for 200 μm as described above. Images were captured at relative depths indicated with the optical system (see Fig. 2B).

Scanning Ion Conductance Microscopy in Vitro

We mapped blood vessels in neural tissue (in vitro) by performing SICM (Sánchez et al. 2008). The pipette was filled with ACSF and pressurized to low positive pressure (30 mbar). First, the pipette was centered above a blood vessel of interest and visualized with a differential interference contrast (DIC) optical system (Olympus, Center Valley, PA). The pipette was manually lowered until the tip resistance increased by 12.5% above initial pipette resistance. The

pipette was then retracted 15 μm and moved laterally to a new, random "grid position." At this new position, the pipette was then moved down 15 μm and the tip resistance was measured again. This process was performed repeatedly until all grid positions were measured. A grid is defined as a square 20 $\mu\text{m} \times 20 \mu\text{m}$ comprising 100 "grid positions" with 2- μm pitch, centered on the initial pipette axial position. The resulting map of resistances as a function of lateral pipette position (at constant depth) was linearly interpolated to 1- μm pitch for visualization and displayed in MATLAB (Natick, MA) as a surface plot (see Fig. 2C).

Regional Pipette Localization in Vivo

RPL (Kodandaramaiah et al. 2012) refers to the act of lowering a pipette into neural tissue to a desired region of interest (e.g., thalamus) under high positive pressure. In our experiments, we performed RPL using two different methods: an uninterrupted, direct, linear trajectory as we have previously described (Kodandaramaiah et al. 2012) and a novel robotic navigation method to avoid obstructions. The method of localization was randomly selected before each trial. A maximum of 10 electrode penetrations were performed per experimental preparation. Pipettes were initially placed on the brain surface under stereoscopic guidance in a region free of large blood vessels.

RPL using linear trajectory. Linear RPL has previously been utilized by us (Kodandaramaiah et al. 2012) and others (Desai et al. 2015) for whole cell electrophysiology in vivo. We used similar parameters; briefly, we applied high positive pressure (1,000 mbar) and translated the pipette at a rate of 500 $\mu\text{m}/\text{s}$. Resistance was recorded during localization as described above, so the resistance array could be displayed and analyzed, at a pitch of 500 $\mu\text{m}/\text{s}/128 \text{ Hz} = 3.9 \mu\text{m}/\text{sample}$.

RPL using robotic navigation. For RPL using robotic navigation, high positive pressure (800 mbar) was applied and the pipette was translated at a rate of 200 $\mu\text{m}/\text{s}$, unless otherwise stated. Resistance was recorded during localization as described above. At the square-wave frequency of 128 Hz, resistance array measurements were spaced 1.6 μm apart. The pipette was inserted along its initial axis, z , at $x, y = (0, 0)$ and moved in x , y , and z to navigate around obstacles.

As shown in Fig. 3, if an obstruction was detected during localization, motion was halted at depth $z_{\text{obstruction}}$ with a pipette resistance of $R_{\text{obstruction}}$ (see Fig. 3, B1 and C). An obstruction detection was defined as follows: pipette resistance increase of at least 12.5% above baseline resistance. Baseline resistance, R_{baseline} , was computed as the

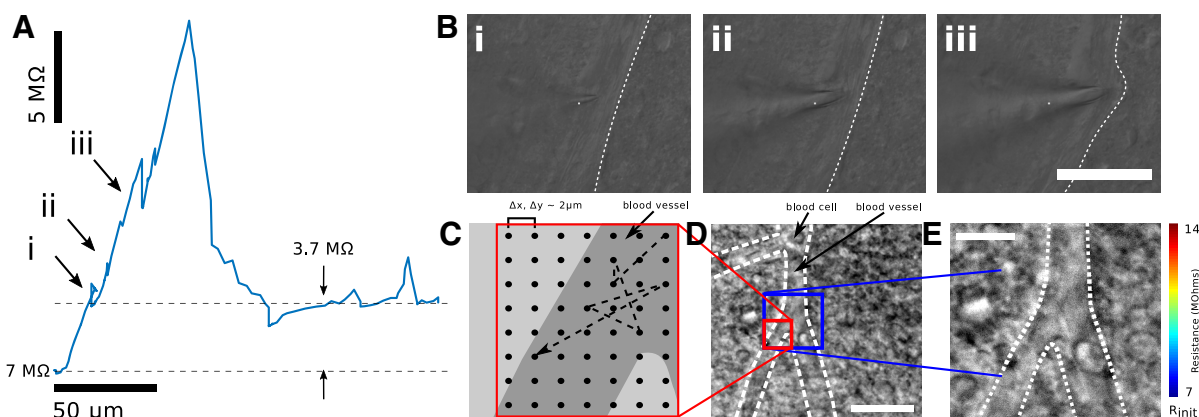


Fig. 2. Lateral navigation around obstructions prevents persistent pipette resistance increase caused by penetration of blood vessels in vitro. **A**: resistance trace as a function of distance as a pipette pierces a blood vessel under high positive pressure. A residual resistance increase of 3.7 $\text{M}\Omega$ remains after the vessel is punctured. **B**: IR DIC images showing the pipette encountering and deforming the blood vessel. Scale bar, 50 μm . **C**: schematic of scanning ion conductance microscopy (SICM) mapping of a blood vessel proceeds from a central point. Samples are collected randomly from a grid area 20 \times 20 μm at 2- μm resolution. **D**: the entire blood vessel and surrounding milieu are shown under IR DIC. Scale bar, 20 μm . **E**: resistances mapped as a function of grid position, clearly showing increased resistance when the pipette is above the blood vessel. Scale bar, 10 μm ; 2 \times interpolation.

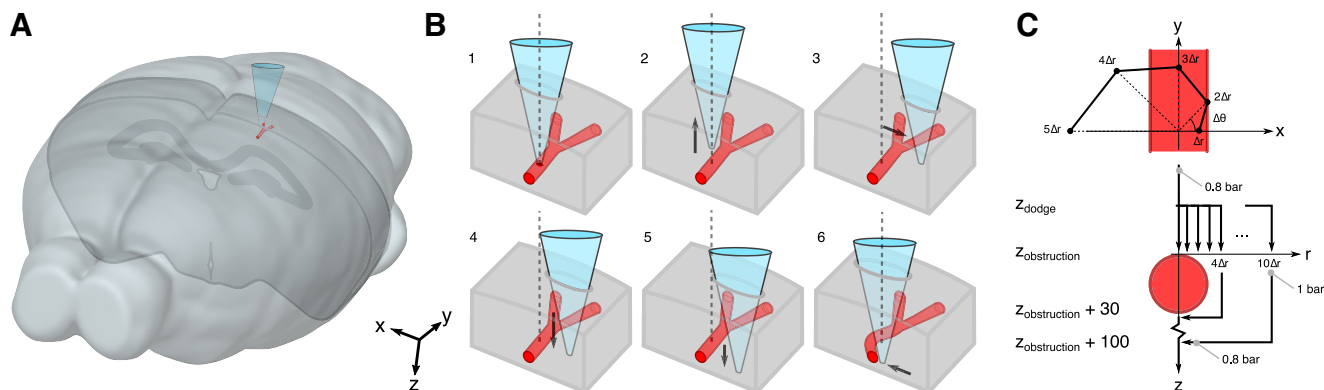


Fig. 3. Robotic navigation algorithm for avoiding blood vessels during regional pipette localization in vivo. *A*: schematic showing vascular avoidance preparation. Brain outline from the Allen Mouse Brain Atlas (Lein et al. 2007). The image was generated with a downloadable application on MacOS. The application can be downloaded at <http://mouse.brain-map.org/static/brainexplorer>. *B*: visual algorithm of vascular avoidance. Obstruction (*I*; here a blood vessel) is detected by an increase in pipette resistance. The pipette is retracted to z_{dodge} (2), moved laterally (3), and advanced to the original $z_{\text{obstruction}}$ (4). If the difference in resistance at $z_{\text{obstruction}}$ and the resistance at z_{dodge} is <200 k Ω , the pipette is advanced through $z_{\text{obstruction}}$ (5) and the pipette is moved back to the original *x*- and *y*-axes (6). *C*: the pipette is navigated around a blood vessel with sequential steps sampling from a spiral pattern. Blood vessel in *A* and *B* shown in isometric view. Blood vessel in *C* shown in top view (*top*) and cross section (*bottom*).

minimum resistance of the previous 800 μm (512 samples from the resistance array, 4 s). With an initial pipette resistance of 4–7 M Ω , 12.5% increase resulted in a minimum $R_{\text{obstruction}}$ of 4.5–7.9 M Ω .

After the motion of the pipette is halted upon obstruction detection, the pipette is moved in a series of steps in an attempt to navigate around the obstruction. First, the pipette is retracted along the pipette axis (*z*) by a distance z_{dodge} (see Fig. 3, *B2* and *C*). The distance z_{dodge} is located relative to $z_{\text{obstruction}}$ within the previous 50 μm (32 samples) at which a minimum pipette resistance, R_{dodge} , was recorded. At depth z_{dodge} , the pipette is moved laterally to dodge, or navigate around, the obstacle that was encountered (see Fig. 3, *B3* and *C*). Lateral movements, centered on the initial pipette axis, are calculated to form a spiral (see Fig. 3*C*) as follows:

$$m(n) = n\Delta r \cos(n\Delta\theta - \pi/4)\mathbf{i} + n\Delta r \sin(n\Delta\theta - \pi/4)\mathbf{j}$$

where $\Delta r = 5$ μm , $\Delta\theta = \pi/4$, and n is the step index {1, 2, 3, ...}. Each step, n , yields a lateral movement vector, m , along which the pipette is moved. The pipette is then lowered back to $z_{\text{obstruction}}$ (see Fig. 3, *B4* and *C*). At $z_{\text{obstruction}}$, the resistance is measured again, termed R_n . If $R_n - R_{\text{dodge}} \geq 200$ k Ω , the obstacle is still in the proximity of the pipette tip and has not been avoided. The pipette is then retracted to z_{dodge} , the step index n is incremented, and another lateral movement occurs. This is repeated until $R_n - R_{\text{dodge}} < 200$ k Ω or until $n = 10$, resulting in a maximum lateral distance of 50 μm .

If $R_n - R_{\text{dodge}} < 200$ k Ω , the obstacle has been successfully avoided. The pipette is advanced 30 μm beyond z_{dodge} to ensure that the obstacle has been passed (see Fig. 3, *B5* and *C*), and then the pipette is moved laterally in a straight line from $x, y = (m_i(n), m_j(n))$ to return to the initial pipette axis, $x, y = (0, 0)$ (see Fig. 3, *B6* and *C*).

Alternatively, if $n = 10$ and $R_n - R_{\text{dodge}} \geq 200$ k Ω , the obstacle was not avoided. In this case, a pulse of high positive pressure (1,000 mbar, 1 s) is applied while the pipette is advanced 100 μm at 200 $\mu\text{m/s}$ to attempt to dislodge the obstruction from the tip of the pipette. The pipette is then moved laterally in a straight line to return to the initial pipette axis, $x, y = (0, 0)$ (see Fig. 3*C*).

Localization is continued until the region of interest is reached and the pipette resistance is <200 k Ω above the baseline resistance, R_b . If the obstruction is not cleared before the end of the region of interest, pipette localization is halted and the pipette is retracted to the surface and replaced.

After successful RPL, the software compensates for pipette capacitance, which is expected to change because of the depth of the recordings discussed here.

RESULTS

RPL Using Linear Trajectory

We have previously developed an automated patch-clamp system, the Autopatcher, and deployed it in the cortex and hippocampus. The results for RPL and yield are shown in Fig. 1, *top*, for depths <1 mm (data from Kodandaramaiah et al. 2012).

To explore the feasibility of using the Autopatcher for whole cell recording in deep subcortical nuclei, we targeted the VPM and surrounding nuclei of the thalamus. The resulting yield of whole cell patching was far below what we observed in our previous cortical patching efforts (see Fig. 1, *top* and *middle*). In 95 trials, one successful whole cell recording was achieved. Furthermore, in 75% of trials (71/95), the pipette reached a depth of 3 mm with a tip resistance above the threshold for removal and replacement. Thus 75% of trials were aborted without attempting gigaseal formation.

To understand what was occurring during linear localization, we modified the Autopatcher so that, as described in MATERIALS AND METHODS, resistance measurement was performed throughout pipette translation, rather than only before and after translation as in our prior work. Consequentially, during linear localization multiple high-amplitude fluctuations of the resistance were revealed, occasionally >25 M Ω (Fig. 4, *A* and *B*). As the pipette advanced, resistance would often return near but not exactly back to baseline, indicating that the event was transient. Final pipette resistance (at the depth of RPL) was on average 730 k Ω greater than the initial resistance measured above the pial surface (Fig. 4*E*). High-amplitude fluctuations were observed in 91% of linear localization trials ($n = 86/95$) (Fig. 4*A*).

Observations of Obstacles

To understand the nature of these high-amplitude resistance fluctuations, we investigated them in vitro, where we could visualize the interaction of the pipette tip with the neural tissue under a microscope. After applying the requisite high positive pressure (1,000 mbar) to a patch pipette, we advanced its tip through the tissue. We noted that the high positive pressure

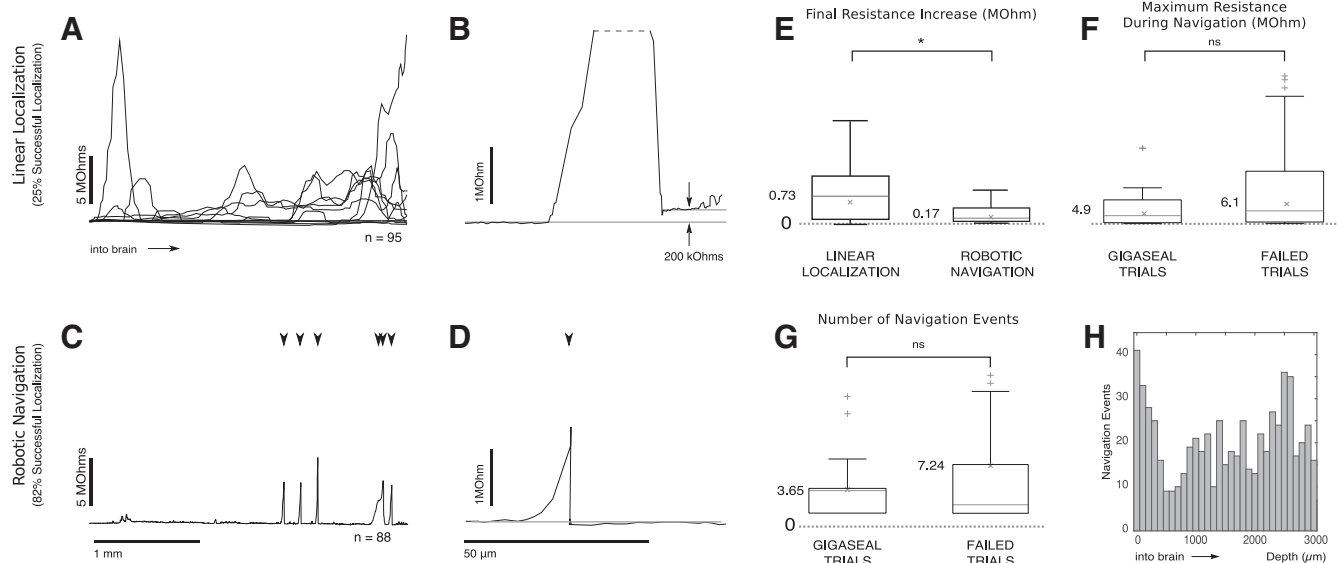


Fig. 4. Pipette tip resistance increases during regional pipette localization in vivo because of accrued debris, preventing whole cell recordings. Robotic navigation prevents this debris from accruing. *A*: recordings of change in pipette resistance during regional pipette localization reveal that obstructions are encountered throughout the insertion path. *B*: when an obstruction is cleared by continuing linear pipette advancement, debris may still be present at the pipette tip, reflected by the persistent resistance increase of the pipette by 200 k Ω . *C*: with a robotic navigation algorithm, pipette debris is prevented from accruing on the pipette tip, shown by the return of the pipette resistance to the baseline. Arrows indicate locations of robotic navigation events. *D*: detail of a single robotic navigation event. *A–D*: initial pipette resistance was subtracted to show changes in resistance. Initial pipette resistances ranged from 4 to 7 M Ω . *E*: the final resistance of the pipette is significantly lower (*) after insertion to 3 mm below the pial surface when the robotic navigation algorithm to localize the pipette was used. *F*: the maximum resistance measured during robotic navigation is not significantly different (ns) between trials that gigasealed successfully ($n = 17$) and trials that failed to seal ($n = 71$), Wilcoxon rank sum test ($P = 0.19$). *G*: the number of navigation events was not significantly different between trials that gigasealed successfully ($n = 17$) and trials that failed to seal ($n = 71$), Wilcoxon rank sum test ($P = 0.96$). *H*: number of navigation events as a function of depth. Note the slight increase in navigation events around 0 μm and 2,500 μm from the pial surface, where the pia and ventricular meninges were encountered, respectively.

easily displaced neurons and glia, but some blood vessels remained in the path of the pipette. As shown in Fig. 2*A*, as the pipette encountered one of these blood vessels during manual axial translation at $\sim 15 \mu\text{m/s}$, the pipette resistance was measured at 10 Hz. The pipette resistance, initially 4.3 M Ω , increased to 26 M Ω within 35 μm as the pipette deformed the blood vessel (Fig. 2*B*). The resistance then quickly decreased as the pipette pierced and passed through the blood vessel. However, a residual blockage was noted, causing an increase in pipette resistance of 3.7 M Ω that persisted until the end of the tissue slice was reached ($\sim 200 \mu\text{m}$). The resistance signature of an obstruction in vitro appears qualitatively similar to resistance fluctuations encountered in vivo (Compare Fig. 2*A* and Fig. 4*B*)—a rapid increase in resistance followed by a rapid decrease, resulting in a residual resistance offset.

The previous result showed the uniaxial (z) signatures of a blood vessel encountered with a pipette. We also mapped blood vessels in neural tissue laterally (x, y) by performing SICM. As shown in Fig. 2, *C–E*, pipette resistance increases were observed over a region that overlapped with the microscopy image of the blood vessel. Concomitantly, regions of tissue adjacent to the blood vessel, populated by neural cells and glia, showed only negligible resistance increases. Additionally, without impaling the blood vessel, no residual increase in resistance was noted even after 100 consecutive resistance measurements. Thus we gained confidence that a blood vessel was the predominant obstacle to pipette insertion in neural tissue and that it could be avoided by moving the pipette laterally even after initial contact if the vessel was not impaled.

Selection of Navigation Algorithm Parameters

We used SICM to further optimize the parameters for encountering, and navigating around, obstacles. We set a threshold for obstacle encounters of 12.5% ($\sim 500 \text{ k}\Omega$); this is greater than the amplitude of baseline resistance variation during localization (100 k Ω) but much less than observed during blood vessel impalement (see Fig. 2*A*).

To determine the axial retraction distance necessary to attempt to dodge an obstacle, z_{dodge} , we first noted that the pipette can drag cells and blood vessels if it is positioned too close to an obstacle. We moved the pipette above a blood vessel and determined the minimum axial retraction distance required to allow a pipette to move laterally without dragging an obstruction to be 15 μm (data not shown). We set a retraction distance of up to $z = 50 \mu\text{m}$ in vivo to ensure that the pipette was safely away from the obstacle before lateral motion, given that the in vivo environment is less predictable than in vitro.

We next attempted to optimize the axial advancement distance necessary to bypass an obstacle after lateral movement. Others have performed a rigorous study of blood vessels in the mouse brain, showing sizes of 10–60 μm (Santisakultarm et al. 2012; Fig. 2*C*). From their data, we compute a mean blood vessel diameter of $28.1 \pm 1.9 \mu\text{m}$. In our observations, capillaries of 15- μm diameter and smaller were easily displaced under high positive pressure. We set a distance of 30 μm to advance the pipette beyond the blood vessel location ($z_{\text{obstruction}}$) to ensure the obstacle had been passed.

Whereas we used 1,000 mbar for RPL during linear localization, we chose a lower pressure (800 mbar) for pipette

insertion during robotic navigation to reduce the volume of ejected intracellular solution during the longer time needed to perform RPL.

To minimize damage to the tissue *in vivo*, we designed the vessel avoidance algorithm to make the smallest lateral and radial movements possible. Radial movement was defined as the distance between the pipette position (x_n, y_n) and the original pipette location at $x, y = (0, 0)$. Lateral distance traveled was defined as the sum of the distances traveled between each point. Movements were made in small increments to minimize radial distance, r , traveled. Additionally, because the orientation of the blood vessel's major axis with respect to the manipulator's x - and y -axes is unknown, we incremented the angle θ with each step, resulting in a spiral search pattern. Similar search patterns have been shown to minimize path length when searching for a line in a two-dimensional plane, analogous to finding the edge of a blood vessel in a plane (Finch and Zhu 2016).

RPL Using Robotic Navigation

Using a robotic navigation algorithm to avoid obstructions during RPL greatly improved the yield of successfully localized pipettes. In 88 trials, 82% of pipettes were localized successfully to a depth of 3,000 μm when the dodging algorithm was active (compared with linear localization, $n = 95$, $P = 7.8448 \times 10^{-15}$, Fisher's exact test). This high yield for RPL using robotic navigation for the thalamus is comparable to rates achieved with RPL using linear trajectories in the cortex.

In addition, the final resistance increase (170 k Ω , $n = 88$) was significantly lower than when the pipette was localized without the algorithm (730 k Ω , $n = 95$, $P = 0.0142$, Wilcoxon rank sum test) (see Fig. 4, *D* and *E*). During robotic navigation, obstructions were encountered in 95% of trials, and on average the dodging algorithm attempted to avoid 6.7 obstructions during each localization (see Fig. 4*C*). At a depth of 3,000 μm , obstructions were therefore encountered every $3,000/6.7 = 445$ μm on average. Each obstruction was successfully avoided in $n = 3.5$ steps, resulting in a radial distance of 17.5 μm on average. RPL under algorithmic guidance was completed in an average of 75 ± 23 s, significantly longer than 6 s (3 mm at 500 $\mu\text{m}/\text{s}$) using the traditional localization method, because of the increased time to avoid obstacles and the lower localization speed. Advantageously, this slow localization may allow tissue to relax before attempting to patch.

The number of robotic navigation events did not have a significant effect on the success of gigasealing. Trials that resulted in a gigaseal ($n = 17$) underwent 3.65 navigation events on average, while trials that failed to result in a gigaseal ($n = 71$) underwent 7.24 navigation events on average ($P = 0.961$ Wilcoxon rank sum test). Additionally, the maximum resistance increase experienced by pipettes during localization did not have an effect on the success of gigasealing. Trials that resulted in a gigaseal ($n = 17$) had an average maximum resistance during localization of 4.9 M Ω , while trials that failed to result in a gigaseal ($n = 71$) had an average maximum resistance during localization of 6.1 M Ω ($P = 0.19$, Wilcoxon rank sum test).

Vertical descent to the thalamus requires penetration of the ventricular meninges, large relatively planar membranes that cannot be avoided with the algorithm described here. The

meninges were routinely detected at ~ 2.5 mm from the pial surface (see Fig. 4*H*). The meninges were penetrated with, on average, 2.3 successive dodge attempts (each resulting in a rapid 100- μm advancement of the pipette).

The yield of whole cell recordings in thalamus improved when RPL was performed with robotic navigation. In trials where whole cell recordings were attempted after RPL with robotic navigation, 10% of trials ($n = 9/88$) resulted in successful whole cell recordings. In trials performed with RPL with linear localization, 1% of trials ($n = 1/95$) resulted in whole cell recordings ($P = 0.0076$, Fisher's exact test).

Whole cell recordings performed in the thalamus with robotic navigation were of quality comparable to those previously performed in the cortex with linear localization (see Fig. 5; Kodandaramaiah et al. 2012; Margrie et al. 2002). Our thalamic recordings had access resistances (32.0 ± 4.1 M Ω) similar to cortical recordings reported by Margrie et al. as well as our prior work, all in the range of 10–50 M Ω (Kodandaramaiah et al. 2012; Margrie et al. 2002). Similarly, our thalamic recordings had holding currents (-50.8 ± 8.9 pA) at -65 -mV holding voltage and resting membrane potentials (-62.9 ± 2.0 mV) that were not significantly different from our previous cortical work: -23.5 ± 12.9 pA ($P = 0.1982$, Wilcoxon rank sum test) and -61.54 ± 1.05 mV ($P = 0.1148$, Wilcoxon rank sum test), respectively.

Recorded neurons had electrophysiological properties consistent with ventrobasal thalamic nucleus neurons, consisting of the VPM and the ventral posterolateral nucleus. In response to hyperpolarizing current injection, sag potentials were observed (hyperpolarization-induced depolarization, indicative of H currents, I_H ; Kuisle et al. 2006; Leist et al. 2016; see Fig. 5*B*). After release of hyperpolarizing currents, burst firing was observed indicative of T-type calcium channel activity, often followed by after (spike) depolarization (Kuisle et al. 2006; Wang et al. 2010b) (see Fig. 5*C*, arrow).

Comparison of whole cell recordings in the thalamus with robotic navigation to those previously reported in the thalamus with linear localization is difficult. There are few reports of successful whole cell thalamic recordings (Brecht and Sakmann 2002; Margrie et al. 2002; Mease et al. 2016; Oberlaender et al. 2012a), and the quality metrics are not reported consistently. However, Margrie et al. (2002) report that "Despite the thalamic recordings being carried out on a younger sample of animals the access resistance was consistently greater than that observed for more superficial recordings." In addition to numerous conversations with other laboratories performing whole cell recordings *in vivo* (personal communications), we assume that the scarcity of published whole cell recordings far below the cortex *in vivo* suggests that they are very difficult to achieve. In our hands, the single cell that was recorded with linear localization during RPL was of lower quality, with an access resistance of 72 M Ω , resting membrane potential of -45 mV, and holding current of -150 pA.

DISCUSSION

Here we describe a method to robotically navigate whole cell patch pipettes through neural tissue *in vivo* in a way that significantly reduces clogging of the tips that occurs commonly when blood vessels are pierced. Pipettes localized without robotic navigation frequently encounter (91% of trials) and

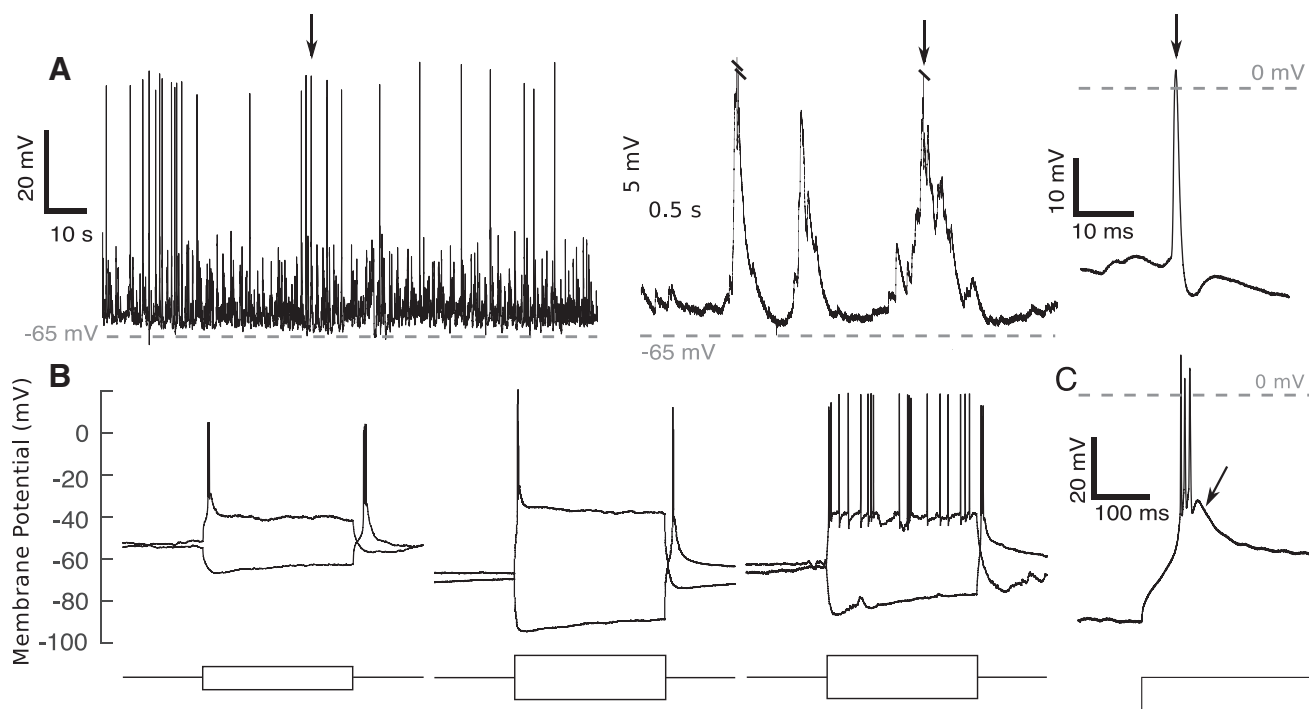


Fig. 5. Neurons recorded in whole cell configuration were of good quality. *A*: example of spontaneous activity from a neuron recorded 3.2 mm below the pial surface with detail of spontaneous burst (arrow indicates burst shown in detail on *right*). *B*: example whole cell traces recorded in the thalamus for 3 different neurons. Note the sag in membrane potential following hyperpolarizing current injection (representing activity of I_h , as described in Leist et al. 2016) and afterhyperpolarization rebound bursting in each trace, indicative of thalamic neurons. Current injections lasted 0.5 s and ranged from ± 50 pA (1st recording) to ± 100 pA (2nd and 3rd recordings). *C*: after hyperpolarizing current injection, rebound bursts exhibited afterdepolarization (see arrow, consistent with ventrobasal thalamic nucleus cells; Wang et al. 2010b). Current injection was -150 pA.

impale obstructions during localization, as others have previously noted (Brecht and Sakmann 2002; Lee et al. 2009; Margrie et al. 2002). This is tolerable for cortical recordings, but as we have shown obstacles are encountered on average every $370 \mu\text{m}$ and therefore make deep, subcortical recordings *in vivo* impractically low in yield and quality.

Previous studies have noted the existence and detrimental effect of permanent resistance increases during RPL (Lee et al. 2014; Margrie et al. 2002), speculating that electrode penetration of the vasculature was the cause (Lee et al. 2014). We have shown, through *in vitro* studies, that these obstructions are very likely caused by encounters with blood vessels larger than $15 \mu\text{m}$. After these encounters, vascular membrane residue adhering to the pipette tip obstructs the tip and increases residual resistance. An efficient spiral navigation algorithm to find the edge of the blood vessel with minimal tissue displacement ($17.5 \mu\text{m}$ on average) enables high-yield RPL.

Robotic navigation enables one to localize pipettes in deep structures (e.g., mouse thalamus at 3 mm) with yields similar to those reported in the cortex with linear localization. Pipettes were successfully localized with robotic navigation to a depth of 3 mm below the pial surface in 82% of trials ($n = 72/88$), comparable to linear localization in the cortex from our previous study (81%, $n = 128/158$, $P = 1$, Fisher's exact test) (Kodandaramaiah et al. 2012).

For whole cell recording yield, there are large ranges of reported yields that make comparison more challenging. Whole cell yield for blind *in vivo* patching has been reported between 20% and 50% (Lee et al. 2009; Margrie et al. 2002), while the yield for two-photon targeted patching in mice *in vivo*

is between 10% and 20% (Margrie et al. 2003). For blind, automated whole cell recording in the mouse cortex, we have previously reported a yield of 31% (Kodandaramaiah et al. 2012). Others have reported yields of 17% (Desai et al. 2015) in mice with similar automation. Our yield of 10% in the mouse thalamus makes recording there practical, although somewhat lower yield than cortical whole cell recording. Additionally, we believe that all subcortical nuclei are now accessible with this method, as electrodes inserted to the VPM must traverse white and gray matter. However, there may still be regions of the brain that may be difficult to access because of their proximity to the ventricles. In this work, we did not address the penetration of the thick ventricular membranes, as such membranes are likely impossible to navigate around and would release CSF into the brain if punctured. Penetration of such membranes remains a problem for maintaining the cleanliness of the electrode but might be mitigated with the application of a reversible, protective coating (Singh et al. 2004). The advent of further automation strategies such as pipette cleaning (Kolb et al. 2016) may further improve the throughput of these experiments.

The whole cell recording yield is the product of the yield of the four stages of the patch algorithm (see Fig. 1). We note a decrease in gigaseal formation yield with deep patching that is irrespective of localization method, linear or robotic. We have observed higher-amplitude heartbeat modulation during the preceding stage, neuron hunting, for the thalamus relative to the cortex, which may indicate greater mechanical disturbances at these depths affecting gigaseal yield. Identifying and overcoming gigaseal yield issues would further advance deep

whole cell patch-clamping efforts and motivate further investigation.

One possible opportunity for improved gigaseal yield is to use the lateral steps performed during SICM to map target cells before gigaseal attempt to optimize the tip placement with respect to the soma, both in vivo and in vitro. Blind in vitro whole cell recordings suffer from low yield (generally 50–80% in vitro; Blanton et al. 1989) compared with image-guided in vitro studies (>80%) (Stuart et al. 1993). Notably, in vitro resistance measurements alone are not sufficient to identify cell membrane dimpling and cell shape, visual identifiers commonly used to align pipettes with target cells for successful gigaseals (Desai et al. 2015). Furthermore, local membrane stiffness, a potential proxy for membrane dimpling, can be estimated by modulating pressure and measuring the difference in tip resistance (Sánchez et al. 2008). The combination of pressure modulation and SICM may improve pipette placement on cell membranes and thereby increase the yield of single-cell experiments in vivo and in vitro.

Leakage of biocytin-containing intracellular solution into the surrounding tissue during RPL may cause background and off-target staining. Intracellular solution in the extracellular space is also undesirable because of the osmotic pressure it places on neurons. This problem may be compounded by the extended time (75 ± 23 s vs. 6 s) spent navigating the pipette through tissue under high positive pressure toward the region of interest. Intracellular solution leakage could be reduced by decreasing the positive pressure during RPL. We hypothesize that a lower pipette pressure during RPL will lead to an increase in obstacle detections as less debris, cells, and blood vessels are displaced by the pipette pressure; however, the optimal pipette pressure was not investigated in this work. Alternatively, cellular contrasts that are not taken up by cells from the extracellular space, such as DNA plasmids, may reduce off-target labeling (Vélez-Fort et al. 2014).

The average number of navigation events (detected obstacles) for trials that eventually successfully formed a gigaseal (3.65) was lower than for trials that eventually failed to form a gigaseal (7.24). While we found that this difference was not statistically significant, we believe the difference in the means is due to the skew of the navigation event distribution. That is, several failed trials resulted from RPL where successive obstacle detections were triggered throughout their descent, either because they were clogged from internal debris or because accrued debris was not successfully dislodged during the navigation events. Although the pipette resistance ultimately returned to baseline in these trials, we suspect that the tip of the pipette may have become contaminated but not measurably clogged. Trials with high numbers of successive obstacle detections may indicate unsuccessful navigation, and the overall success rate may improve with rejection of these trials.

Intracellular recording has remained the gold standard electrophysiology technique because of its high quality, mechanical stability, and resolution. Margrie et al. hypothesized that pipette contamination results in higher access resistances and thus lower-quality thalamic recordings. Previous efforts to reduce the access resistance of recordings performed deep in the brain by using higher pressures in the pipette or a guide tube have not been successful (Brecht and Sakmann 2002). Here we demonstrate that robotic navigation around blood vessels in vivo results in not only higher yield than with linear

localization but also higher-quality recordings. Critically, we demonstrate that robotic navigation during RPL produces whole cell recordings 3 mm below the pial surface with access resistances similar to those measured from cells in the cortex (Kodandaramaiah et al. 2012; Margrie et al. 2002). Other factors may contribute to differences in yield and access resistance, namely pipette shape and tip geometry, but these parameters are rarely reported or quantified, making comparison difficult. Other parameters were also comparable to previous recordings in cortex, including holding current (voltage clamp, used to keep the cell at -65 mV) and resting membrane potential (Kodandaramaiah et al. 2012). Thus we are confident that in vivo whole cell recording quality is improved from previous efforts to perform whole cell recordings in the thalamus and is equivalent to recordings in the cortex.

There are very few published studies that show in vivo whole cell recordings at depths 3 mm or greater. In fact, to our knowledge, only seven such studies have been published to date (Brecht and Sakmann 2002; Groh et al. 2014; Kuo and Wu 2012; Margrie et al. 2002; Mease et al. 2016; Oberlaender et al. 2012a, 2012b). In contrast, in vitro whole cell recordings in deep subcortical nuclei are abundant (Benavides et al. 2007; Guo et al. 2012; Hu et al. 2008; Kase et al. 2012; Neuhoff et al. 2002; Porcello et al. 2002; Sosulina et al. 2010). This indicates that there is interest in performing high-yield subcortical whole cell recordings in vivo, while recording depth is an impediment for whole cell studies in these nuclei. Additionally, the whole cell patch-clamp technique is uniquely positioned to investigate the structure-function-gene relationship (Cadwell et al. 2016). This study opens the door for whole cell electrophysiology coupled with genetic or morphological profiling throughout the entire brain, which is the focus of worldwide effort (Cadwell et al. 2016; Hawrylycz et al. 2016; Oberlaender et al. 2012a; Vélez-Fort et al. 2014) and a major goal of the BRAIN Initiative (Bargmann and Newsome 2014).

GRANTS

This work was funded by National Institutes of Health Grants 1U01 MH-106027 (W. A. Stoy, Y. Liew, G. B. Stanley, C. R. Forest), 1R01 EY-023173 (G. Holst, E. S. Boyden, C. R. Forest), R01 NS-048285 (G. B. Stanley), R01 NS-085447 (G. B. Stanley), and T90 DA-032466 (I. Kolb).

DISCLOSURES

No conflicts of interest, financial or otherwise, are declared by the authors.

AUTHOR CONTRIBUTIONS

W.A.S., I.K., G.H., and C.R.F. conceived and designed research; W.A.S. performed experiments; W.A.S. analyzed data; W.A.S., I.K., Y.L., A.P., B.Y., G.B.S., and C.R.F. interpreted results of experiments; W.A.S. prepared figures; W.A.S. and C.R.F. drafted manuscript; W.A.S., I.K., G.H., Y.L., A.P., B.Y., E.S.B., G.B.S., and C.R.F. edited and revised manuscript; W.A.S., I.K., G.H., Y.L., A.P., B.Y., E.S.B., G.B.S., and C.R.F. approved final version of manuscript.

REFERENCES

- Bargmann C, Newsome W. *BRAIN 2025: a Scientific Vision*. Bethesda, MD: National Institutes of Health, 2014.
- Benavides DR, Quinn JJ, Zhong P, Hawasli AH, DiLeone RJ, Kansy JW, Olausson P, Yan Z, Taylor JR, Bibb JA. Cdk5 modulates cocaine reward, motivation, and striatal neuron excitability. *J Neurosci* 27: 12967–12976, 2007. doi:10.1523/JNEUROSCI.4061-07.2007.

- Blanton MG, Lo Turco JJ, Kriegstein AR. Whole cell recording from neurons in slices of reptilian and mammalian cerebral cortex. *J Neurosci Methods* 30: 203–210, 1989. doi:10.1016/0165-0270(89)90131-3.
- Brecht M, Sakmann B. Whisker maps of neuronal subclasses of the rat ventral posterior medial thalamus, identified by whole-cell voltage recording and morphological reconstruction. *J Physiol* 538: 495–515, 2002. doi:10.1113/jphysiol.2001.012334.
- Cadwell CR, Palasantza A, Jiang X, Berens P, Deng Q, Yilmaz M, Reimer J, Shen S, Bethge M, Tolias KF, Sandberg R, Tolias AS. Electrophysiological, transcriptomic and morphologic profiling of single neurons using Patch-seq. *Nat Biotechnol* 34: 199–203, 2016. doi:10.1038/nbt.3445.
- Constantinople CM, Bruno RM. Deep cortical layers are activated directly by thalamus. *Science* 340: 1591–1594, 2013. doi:10.1126/science.1236425.
- Desai NS, Siegel JJ, Taylor W, Chitwood RA, Johnston D. MATLAB-based automated patch-clamp system for awake behaving mice. *J Neurophysiol* 114: 1331–1345, 2015. doi:10.1152/jn.00025.2015.
- Fee MS. Active stabilization of electrodes for intracellular recording in awake behaving animals. *Neuron* 27: 461–468, 2000. doi:10.1016/S0896-6273(00)00057-X.
- Finch SR, Zhu LY. Searching for a Shoreline. arXiv.org. math/0501123v2, 2016.
- Friedberg MH, Lee SM, Ebner FF. The contribution of the principal and spinal trigeminal nuclei to the receptive field properties of thalamic VPM neurons in the rat. *J Neurocytol* 33: 75–85, 2004. doi:10.1023/B:NEUR.0000029649.28599.a5.
- Groh A, Bokor H, Mease RA, Plattner VM, Hangya B, Stroh A, Deschênes M, Acsády L. Convergence of cortical and sensory driver inputs on single thalamocortical cells. *Cereb Cortex* 24: 3167–3179, 2014. doi:10.1093/cercor/bht173.
- Guo ML, Xue B, Jin DZ, Liu ZG, Fibuch EE, Mao LM, Wang JQ. Upregulation of Npas4 protein expression by chronic administration of amphetamine in rat nucleus accumbens in vivo. *Neurosci Lett* 528: 210–214, 2012. doi:10.1016/j.neulet.2012.07.048.
- Harvey CD, Collman F, Dombeck DA, Tank DW. Intracellular dynamics of hippocampal place cells during virtual navigation. *Nature* 461: 941–946, 2009. doi:10.1038/nature08499.
- Hawrylycz M, Anastassiou C, Arhipov A, Berg J, Buice M, Cain N, Gouwens NW, Gratiy S, Iyer R, Lee JH, Mihalas S, Mitelut C, Olsen S, Reid RC, Teeter C, de Vries S, Waters J, Zeng H, Koch C; MindScope. Inferring cortical function in the mouse visual system through large-scale systems neuroscience. *Proc Natl Acad Sci USA* 113: 7337–7344, 2016. doi:10.1073/pnas.1512901113.
- Higley MJ, Contreras D. Cellular mechanisms of suppressive interactions between somatosensory responses in vivo. *J Neurophysiol* 97: 647–658, 2007. doi:10.1152/jn.00777.2006.
- Hu XT, Nasif FJ, Zhang J, Xu M. Fos regulates neuronal activity in the nucleus accumbens. *Neurosci Lett* 448: 157–160, 2008. doi:10.1016/j.neulet.2008.10.025.
- Kase D, Inoue T, Imoto K. Roles of the subthalamic nucleus and subthalamic HCN channels in absence seizures. *J Neurophysiol* 107: 393–406, 2012. doi:10.1152/jn.00937.2010.
- Kelly ST, Kremkow J, Jin J, Wang Y, Wang Q, Alonso JM, Stanley GB. The role of thalamic population synchrony in the emergence of cortical feature selectivity. *PLoS Comput Biol* 10: e1003418, 2014. doi:10.1371/journal.pcbi.1003418.
- Kodandaramaiah SB, Franzesi GT, Chow BY, Boyden ES, Forest CR. Automated whole-cell patch-clamp electrophysiology of neurons in vivo. *Nat Methods* 9: 585–587, 2012. doi:10.1038/nmeth.1993.
- Kodandaramaiah SB, Holst GL, Wickersham IR, Singer AC, Franzesi GT, McKinnon ML, Forest CR, Boyden ES. Assembly and operation of the autopatcher for automated intracellular neural recording in vivo. *Nat Protoc* 11: 634–654, 2016. doi:10.1038/nprot.2016.007.
- Kolb I, Stoy WA, Rousseau EB, Moody OA, Jenkins A, Forest CR. Cleaning patch-clamp pipettes for immediate reuse. *Sci Rep* 6: 35001, 2016. doi:10.1038/srep35001.
- Kuise M, Wanaverbecq N, Brewster AL, Frère SG, Pinault D, Baram TZ, Lüthi A. Functional stabilization of weakened thalamic pacemaker channel regulation in rat absence epilepsy. *J Physiol* 575: 83–100, 2006. doi:10.1113/jphysiol.2006.110486.
- Kuo RI, Wu GK. The generation of direction selectivity in the auditory system. *Neuron* 73: 1016–1027, 2012. doi:10.1016/j.neuron.2011.11.035.
- Lee AK, Epsztein J, Brecht M. Head-anchored whole-cell recordings in freely moving rats. *Nat Protoc* 4: 385–392, 2009. doi:10.1038/nprot.2009.5.
- Lee D, Shtengel G, Osborne JE, Lee AK. Anesthetized- and awake-patched whole-cell recordings in freely moving rats using UV-cured collar-based electrode stabilization. *Nat Protoc* 9: 2784–2795, 2014. doi:10.1038/nprot.2014.190.
- Lein ES, Hawrylycz MJ, Ao N, Ayres M, Bensinger A, Bernard A, Boe AF, Boguski MS, Brockway KS, Byrnes EJ, Chen L, Chen L, Chen TM, Chin MC, Chong J, Crook BE, Czaplinska A, Dang CN, Datta S, Dee NR, Desaki AL, Desta T, Diep E, Dolbeare TA, Donelan MJ, Dong HW, Dougherty JG, Duncan BJ, Ebbert AJ, Eichele G, Estlin LK, Faber C, Facer BA, Fields R, Fischer SR, Fliss TP, Frensley C, Gates SN, Geffardtler KJ, Halverson KR, Hart MR, Hohmann JG, Howell MP, Jeung DP, Johnson RA, Karr PT, Kawal R, Kidney JM, Knapik RH, Kuan CL, Lake JH, Laramée AR, Larsen KD, Lau C, Lemon TA, Liang AJ, Liu Y, Luong LT, Michaels J, Morgan JJ, Morgan RJ, Mortrud MT, Mosqueda NF, Ng LL, Ng R, Orta GJ, Overly CC, Pak TH, Parry SE, Pathak SD, Pearson OC, Puchalski RB, Riley ZL, Rockett HR, Rowland SA, Royall JJ, Ruiz MJ, Sarno NR, Schaffnit K, Shapovalova NV, Sivisay T, Slaughterbeck CR, Smith SC, Smith KA, Smith BI, Sodt AJ, Stewart NN, Stumpf KR, Sunkin SM, Sutram M, Tam A, Teemer CD, Thaller C, Thompson CL, Varnam LR, Visel A, Whitlock RM, Wohnoutka PE, Wolkey CK, Wong VY, Wood M, Yaylaoglu MB, Young RC, Youngstrom BL, Yuan XF, Zhang B, Zwingman TA, Jones AR. Genome-wide atlas of gene expression in the adult mouse brain. *Nature* 445: 168–176, 2007.
- Leist M, Datunashvili M, Kanyshkova T, Zobeiri M, Aissaoui A, Cerina M, Romanelli MN, Pape HC, Budde T. Two types of interneurons in the mouse lateral geniculate nucleus are characterized by different h-current density. *Sci Rep* 6: 24904, 2016. doi:10.1038/srep24904.
- Lin MZ, Schnitzer MJ. Genetically encoded indicators of neuronal activity. *Nat Neurosci* 19: 1142–1153, 2016. doi:10.1038/nn.4359.
- Llinás RR, Steriade M. Bursting of thalamic neurons and states of vigilance. *J Neurophysiol* 95: 3297–3308, 2006. doi:10.1152/jn.00166.2006.
- Margrie TW, Brecht M, Sakmann B. In vivo, low-resistance, whole-cell recordings from neurons in the anaesthetized and awake mammalian brain. *Pflügers Arch* 444: 491–498, 2002. doi:10.1007/s00424-002-0831-z.
- Margrie TW, Meyer AH, Caputi A, Monyer H, Hasan MT, Schaefer AT, Denk W, Brecht M. Targeted whole-cell recordings in the mammalian brain in vivo. *Neuron* 39: 911–918, 2003. doi:10.1016/j.neuron.2003.08.012.
- Mease RA, Sumser A, Sakmann B, Groh A. Cortical dependence of whisker responses in posterior medial thalamus in vivo. *Cereb Cortex* 26: 3534–3543, 2016. doi:10.1093/cercor/bhw144.
- Neher E. Ion channels for communication between and within cells In: *Nobel Lectures—Physiology or Medicine, 1991–1995*, edited by Ringertz N. Singapore: World Scientific, 1997.
- Neuhoff H, Neu A, Liss B, Roeper J. I_h channels contribute to the different functional properties of identified dopaminergic subpopulations in the mid-brain. *J Neurosci* 22: 1290–1302, 2002.
- Oberlaender M, de Kock CP, Bruno RM, Ramirez A, Meyer HS, Dercksen VJ, Helmstaedter M, Sakmann B. Cell type-specific three-dimensional structure of thalamocortical circuits in a column of rat vibrissal cortex. *Cereb Cortex* 22: 2375–2391, 2012a. doi:10.1093/cercor/bhr317.
- Oberlaender M, Ramirez A, Bruno RM. Sensory experience restructures thalamocortical axons during adulthood. *Neuron* 74: 648–655, 2012b. doi:10.1016/j.neuron.2012.03.022.
- Paxinos G, Franklin KB. *The Mouse Brain in Stereotaxic Coordinates*. San Diego, CA: Academic, 2012.
- Petersen RS, Brambilla M, Bale MR, Alenda A, Panzeri S, Montemurro MA, Maravall M. Diverse and temporally precise kinetic feature selectivity in the VPM thalamic nucleus. *Neuron* 60: 890–903, 2008. doi:10.1016/j.neuron.2008.09.041.
- Polack PO, Champier S. Intracellular activity of cortical and thalamic neurons during high-voltage rhythmic spike discharge in Long-Evans rats in vivo. *J Physiol* 571: 461–476, 2006. doi:10.1113/jphysiol.2005.100925.
- Porcello DM, Ho CS, Joho RH, Huguenard JR. Resilient RTN fast spiking in Kv3.1 null mice suggests redundancy in the action potential repolarization mechanism. *J Neurophysiol* 87: 1303–1310, 2002. doi:10.1152/jn.00556.2001.
- Rancz EA, Franks KM, Schwarz MK, Pichler B, Schaefer AT, Margrie TW. Transfection via whole-cell recording in vivo: bridging single-cell physiology, genetics and connectomics. *Nat Neurosci* 14: 527–532, 2011. doi:10.1038/nn.2765.
- Sánchez D, Johnson N, Li C, Novak P, Rheinlaender J, Zhang Y, Anand U, Anand P, Gorelik J, Frolenkov GI, Benham C, Lab M, Ostanin VP,

- Schäffer TE, Klenerman D, Korchev YE.** Noncontact measurement of the local mechanical properties of living cells using pressure applied via a pipette. *Biophys J* 95: 3017–3027, 2008. doi:10.1529/biophysj.108.129551.
- Santisakultarm TP, Cornelius NR, Nishimura N, Schafer AI, Silver RT, Doerschuk PC, Olbricht WL, Schaffer CB.** In vivo two-photon excited fluorescence microscopy reveals cardiac- and respiration-dependent pulsatile blood flow in cortical blood vessels in mice. *Am J Physiol Heart Circ Physiol* 302: H1367–H1377, 2012. doi:10.1152/ajpheart.00417.2011.
- Sherman SM.** The role of the thalamus in cortical function: not just a simple relay. *Thalamus Relat Syst* 3: 205–216, 2005. doi:10.1017/S1472928807000210.
- Singh A, Zhu H, He J.** Improving mechanical stiffness of coated benzocyclobutene (BCB) based neural implant. *Conf Proc IEEE Eng Med Biol Soc* 6: 4298–4301, 2004. doi:10.1109/IEMBS.2004.1404197.
- Sosulina L, Graebenitz S, Pape HC.** GABAergic interneurons in the mouse lateral amygdala: a classification study. *J Neurophysiol* 104: 617–626, 2010. doi:10.1152/jn.00207.2010.
- Stuart GJ, Dodt HU, Sakmann B.** Patch-clamp recordings from the soma and dendrites of neurons in brain slices using infrared video microscopy. *Pflügers Arch* 423: 511–518, 1993. doi:10.1007/BF00374949.
- Vélez-Fort M, Rousseau CV, Niedworok CJ, Wickersham IR, Rancz EA, Brown AP, Strom M, Margrie TW.** The stimulus selectivity and connectivity of layer six principal cells reveals cortical microcircuits underlying visual processing. *Neuron* 83: 1431–1443, 2014 [Erratum. *Neuron* 84: 238, 2014]. doi:10.1016/j.neuron.2014.08.001.
- Wang Q, Webber RM, Stanley GB.** Thalamic synchrony and the adaptive gating of information flow to cortex. *Nat Neurosci* 13: 1534–1541, 2010a. doi:10.1038/nn.2670.
- Wang X, Vaingankar V, Soto Sanchez C, Sommer FT, Hirsch JA.** Thalamic interneurons and relay cells use complementary synaptic mechanisms for visual processing. *Nat Neurosci* 14: 224–231, 2011. doi:10.1038/nn.2707.
- Wang X, Wei Y, Vaingankar V, Wang Q, Koepsell K, Sommer FT, Hirsch JA.** Feedforward excitation and inhibition evoke dual modes of firing in the cat's visual thalamus during naturalistic viewing. *Neuron* 55: 465–478, 2007. doi:10.1016/j.neuron.2007.06.039.
- Wang X, Yu G, Hou X, Zhou J, Yang B, Zhang L.** Rebound bursts in GABAergic neurons of the thalamic reticular nucleus in postnatal mice. *Physiol Res* 59: 273–280, 2010b.
- Wu Q, Kolb I, Callahan BM, Su Z, Stoy W, Kodandaramaiah SB, Neve R, Zeng H, Boyden ES, Forest CR, Chubykin AA.** Integration of autpatching with automated pipette and cell detection in vitro. *J Neurophysiol* 116: 1564–1578, 2016. doi:10.1152/jn.00386.2016.
- Yu YQ, Xiong Y, Chan YS, He J.** Corticofugal gating of auditory information in the thalamus: an in vivo intracellular recording study. *J Neurosci* 24: 3060–3069, 2004. doi:10.1523/JNEUROSCI.4897-03.2004.

